A Study of the Propagation of Turbulent Premixed Flame Using the Flame Surface Density Model in a Constant Volume Combustion Chamber

Kyungwon Yun
Hyundai Motor Company
Sangsu Lee*
Graduate School of Mechanical Engineering, Sungkyunkwan University, Kyunggi-do 440-746, Korea
Nakwon Sung
School of Mechanical Engineering, Sungkyunkwan University, Kyunggi-do 440-746, Korea

Three-dimensional numerical analysis of the turbulent premixed flame propagation in a constant volume combustion chamber is performed using the KIVA-3V code (Amsden et. al. 1997) by the flame surface density (FSD) model. A simple near-wall boundary condition is eaployed to describe the interaction between turbulent premixed flame and the wall. A mean stretch factor is introduced to include the stretch and curvature effects of turbulence. The results from the FSD model are compared with the experimental results of schlieren photos and pressure measurements. It is found that the burned mass rate and flame propagation by the FSD model are in reasonable agreement with the experimental results. The FSD combustion model proved to be effective for description of turbulent premixed flames.

Key Words : Turbulent Premixed Flame, Constant Volume Combustion Chamber, Flame Propagation, Flame Surface Density Model

1. Introduction

Computational fluid dynamics has been used to study the combustion in gas burners, spark-ignition engines and low NOx gas turbines. Recently, the eddy break up (EBU) model, the probability density function (PDF) model and the flame surface density (FSD) model have been suggested for modeling turbulent premixed flames. The EBU model assumes that the mean reaction rate is controlled by the turbulent mixing time with no consideration for chemical reaction effects. The basic advantage of the PDF model for turbulent reaction flow is that it does not require modeling of the nonlinear chemical source term.

The FSD model assumes that chemical reaction occurs in thin layers called flamelets. This regime of combustion prevails when the chemical time scales are smaller than the turbulence time scales. In the current study, the generalized flamelet assumption, which requires that chemical reactions take place in a collection of thin sheets propagating at the laminar flame speed, is adopted. The FSD model has the advantage that the influences of chemical reaction and turbulent effect are treated separately.

Marble and Broadwell (1977) introduced a concept of the FSD model. The flame surface density equations were proposed by Cant et. al. (1990), Duclos et. al. (1993), Mantel and Borghi (1994), Cheng and Diringer (1991), and Choi and Huh(1998). Cheng and Diringer (1991) proposed a simplified FSD combustion model

* Corresponding Author,
E-mail : sangsu@nature.skku.ac.kr
TEL : +82-31-290-7498; **FAX** : +82-31-290-7498
Graduate School of Mechanical Engineering, Sungkyunkwan University, Kyunggi-do, Korea. (Manuscript **Received** September 22, 2001; **Revised** January 11, 2002)

and analyzed the turbulent flame propagation in a spark-ignition engine using the KIVA-II code. Cheng's equation neglected the strain rate due to mean flow and showed unphysical acceleration of the flame near the cylinder wall.

In this paper, Cheng's FSD model was modified to consider the effects of wall quenching in the boundary layer and to predict flame propagation in a constant volume combustion chamber.

2. The Turbulent Premixed Combustion Model

The FSD model assumes wrinkled laminar flamelets as shown in Fig. 1. The model calculates the average reaction rate in terms of the stretched flame area, which in turn, depends on turbulent flow and laminar flame velocity. The effects of turbulence are wrinkling flame fronts to increase the flame area. The mass burning rate in turbulent premixed flame can be calculated in terms of the laminar flame speed and the increased flame area in the wrinkled flame regime as,

$$\dot{m}=\rho_u S_t \bar{A}=\rho_u S_L A_{flame}. \tag{1}$$

The flame surface density is defined as,

$$\Sigma=\frac{A_{flame}}{V}. \tag{2}$$

The time-averaged reaction rate in a unit volume is given by

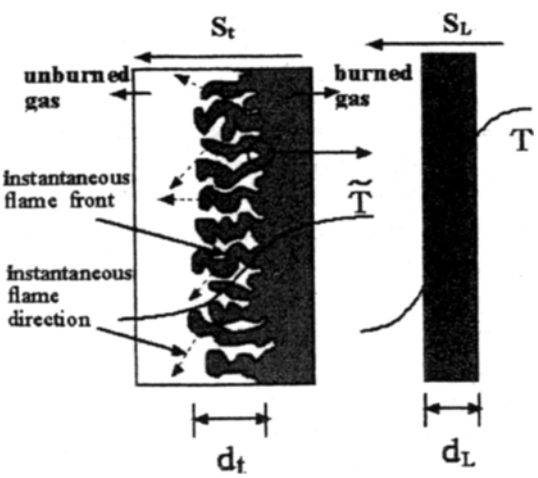

Fig. 1 Wrinkled laminar flamelet approximation

$$\bar{\dot{w}}=\rho_u I_0 S_L \Sigma \tag{3}$$

where ρ_u is the density of the unburned gas, I_0 a mean stretch factor and S_L the laminar flame speed. S_L is calculated from Metghalchi and Keck (1996)'s data. I_0 represents the effects of the strain rate and the radius of curvature acting on the laminar flamelets on the time-averaged reaction rate. I_0 is defined as the ratio of the average laminar flame speed to the unstretched laminar flame speed. I_0 is calculated from Bray (1994)s equation which employs Markstein number M_c and Karlovitz number K_a is

$$I_0=1-0.28 M_c K_a \tag{4}$$

where, Markstein Number is defined as

$$M_c=\left(\frac{1+\phi}{\phi}\right)\ln(1+\phi) \tag{5}$$

where $\phi=\frac{T_b}{T_u}-1$, T_b is burned gas temperature and T_u is unburned gas temperature. T_u and T_b are calculated using an ideal gas state equation.

Karlovitz Number, on the other hand, is used to determine whether the flame is extinguishable.

$$K_a=\left(\frac{u'}{l_\lambda}\right)\left(\frac{\delta_L}{S_L}\right) \tag{6}$$

where u' is the turbulent intensity, l_λ the Taylor microscale, and δ_L the laminar flame thickness.

The turbulent Reynolds number and Damkohler number is useful for determining the flames combustion regime. The turbulent Reynolds number is

$$Re_t=\frac{u' l}{\nu} \tag{7}$$

where l is the integral length scale.

The Damkohler number is the ratio of large scale eddies to the transit time of the laminar flamelet.

$$Da=\left(\frac{l}{u'}\right)\Big/\left(\frac{\delta_l}{S_L}\right) \tag{8}$$

The flame surface density equation used is from Cheng's equation, except modification of a near-wall source term.

$$\frac{D\Sigma}{Dt}+\nabla\cdot(u\Sigma)=\frac{1}{\rho}\nabla\cdot(\rho D_\Sigma \nabla\Sigma)$$

$$+s\Sigma-\frac{\beta\rho_u S_L\Sigma}{\rho Y_1}$$

$$s=\begin{cases} +\ ae & \text{for } e<e_s \\ -\eta(e-e_s) & \text{for } e>e_s \\ +\ e_w & \text{for } wall \end{cases} \tag{9}$$

The unsteady term and the convective term on the left hand side of Eq. (9) have the same form as the species conservation equation in KIVA-3V. The terms on the right hand side are a diffusion term, a production term, and a destruction term. e is the average strain rate and calculated from the turbulence model. From the dimensional analysis of k-ε turbulence model,

$$e=Ce\frac{\varepsilon}{k} \tag{10}$$

where Ce is fixed at 5.

When the strain rate is less than the critical value, e_c,

$$e_c=K_a S_L/\delta \tag{11}$$

it is assumed that the generation rate of the flame surface is proportional to the local average magnitude of the strain rate e with a proportional constant a in the order of 1 to 10. When the strain rate exceeds e_c, the flame surface may be locally extinguished by overstraining of the fluid element. The flame surface extinction rate is proportional to the amount of overstraining.

When using turbulence model such as the k-ε model, underestimation of the turbulent kinetic energy and overestimation of the dissipation rate occur in the vicinity of the wall. In order to correct this problem the strain rate at the wall is modified considering wall quenching and the boundary layer,

$$e_w=\gamma_w\left(\frac{\rho_u}{\rho_b}\right)\left(\frac{S_L}{l_w}\right) \tag{12}$$

The strain rate at the wall is modeled from the phenomenological description. In the vicinity of the wall, the strain rate is evaluated from the burned gas properties, the laminar burning speed, and the distance from the wall. In contrast with the strain rate at the wall from the k-ε model, the flame propagation speed near the wall is greatly decreased during propagation.

The last term in Eq. (9) takes care of destruction of the flame density by burning, and β is the proportional constant determined by experimentation.

The transport equation of the flame surface density is rewritten by a pseudo species variable, $\zeta=\rho\Sigma$

$$\frac{\partial\zeta}{\partial t}+\nabla\cdot(u\zeta)=\nabla\cdot[\rho D_\Sigma\nabla(\zeta/\rho)] +s\zeta-\frac{\beta\rho_u S_L\zeta^2}{\rho^2 Y_1}-(\nabla\cdot u)\zeta \tag{13}$$

In Eq. (13), the convective term in the left hand side and the diffusive term in the right hand side are solved using the algorithms in the KIVA-3V. The remaining terms are coded into KIVA code and solved by the following equation.

$$F(\zeta)=s\zeta-\frac{\beta\rho_u S_L\zeta^2}{\rho^2 Y_1}-(\nabla\cdot u)\zeta \tag{14}$$

The solution of the above equation is

$$\zeta(t+\delta t)=\frac{a\zeta(t)}{b\zeta(t)(1-e^{-a\delta t})+ae^{-a\delta t}}$$

$$a=s-\nabla\cdot u=\begin{bmatrix} +\ ae \\ -\eta(e-e_s) \\ +\ e_w \end{bmatrix}-\nabla\cdot u$$

$$b=\frac{\beta\rho_u S_L}{\rho^2 Y_1} \tag{15}$$

The spark ignition gives the initial condition for the flame density. A flame kernel produced near the spark plug during ignition grows at the laminar flame speed during 1ms of ignition time.

$$R(t)=S_L(t-t_{ign})\frac{T_b}{T_u}+R_0 \tag{16}$$

Now, ζ can be calculated as follows.

$$\zeta_{ignition}=\rho\Sigma_{ignition}=\rho 4\pi R^2/V \tag{17}$$

where R_0 is the initial flame radius and its typical value 0.5mm was proposed by Cheng et. al. (1991).

Fig. 2 is a schematic diagram of the constant volume combustion chamber used in this study. The cylindrical chamber is 80mm in diameter and 25mm in height. The ignition is initiated at the center of the wall. In order to find the sensitivity of the grid size on the solution, three different meshes were tested. The volumes of a cell in each case were 8.7mm^3, 3.65mm^3 and 2.04mm^3 respec-

Table 1 Calculation conditions

Swirl flow strength (Re_pNO.)	1950, 3435, 6313
Initial temperature (K)	313
Initial pressure (bar)	1
Equivalence ratio	1.0
Fuel	C_3H_8

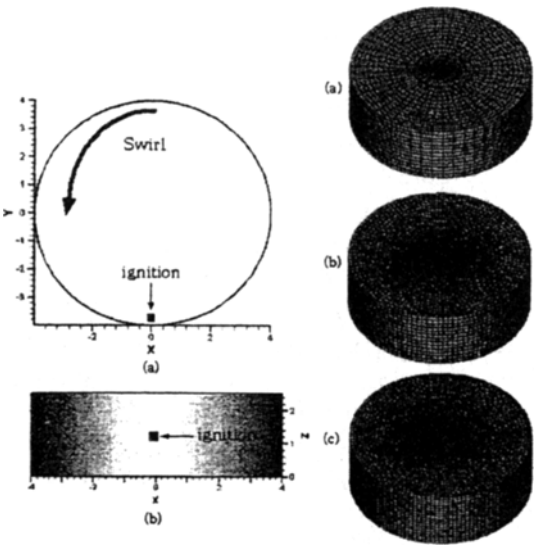

Fig. 2 Schematic diagram of the constant volume combustion chamber and the meshes used for the calculations

tively.

The calculation conditions are listed in Table 1. The swirl flow strength is defined by $Re_P = RU/v$, where R is the distance from the center of combustion chamber to the position of ignition, and U and v denote mean velocity and kinetic viscosity coefficient, respectively. The counterclockwise swirl intensity of fluid is given by the initial velocity field of KIVA-3V. $Re_P = 3435$ is selected as the baseline condition.

3. Results and Discussion

3.1 FSD combustion model

The results from the different grid sizes are shown in Fig. 3. The bigger grid results in the fast

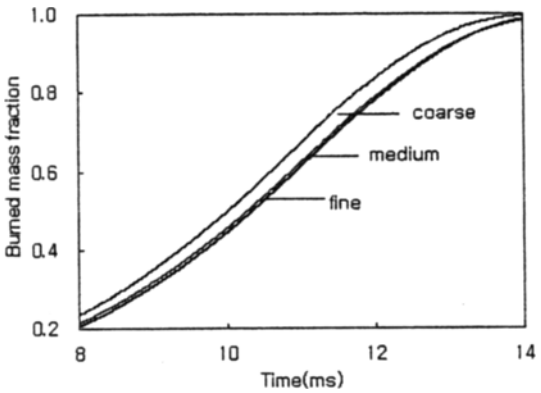

Fig. 3 Effect of the computational grid resolution on pressure history and burned mass fraction

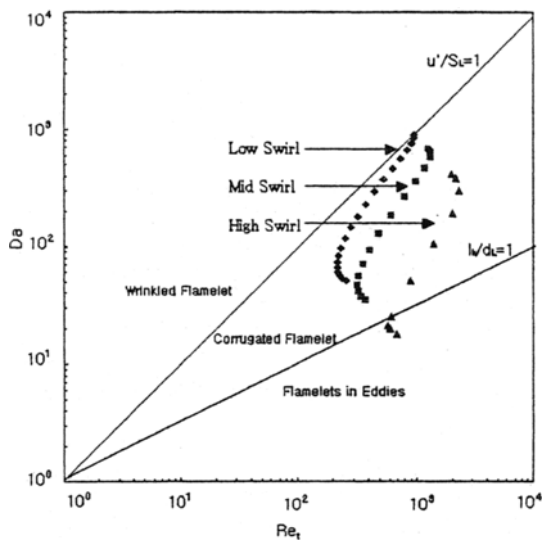

Fig. 4 The turbulent combustion regimes for the three swirl strengths

burn-rate because of the increased flame surface. When the grid size becomes smaller, as in the case of the medium and fine resolution cases, the results obtained from the simulations are similar. The computation times used for three different meshes are 3hours, 15hours, and 22 hours, respectively. For the efficiency of the calculation, the medium grid was selected in this study.

The regimes of the turbulent premixed combustion in this study were evaluated. Figure 4 shows the turbulent combustion regimes in terms of the Reynolds number and Damkohler number. As the flame propagates, the Damkohler number

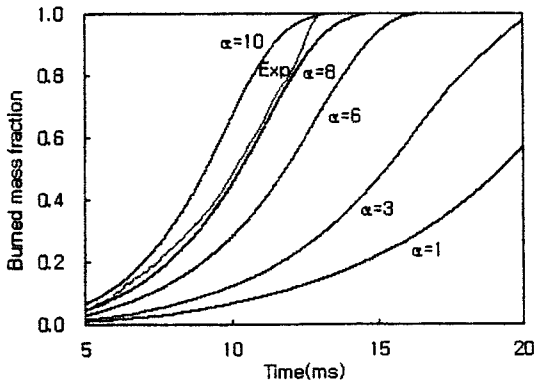

Fig. 5 Effect of the parameter α on burned mass fraction

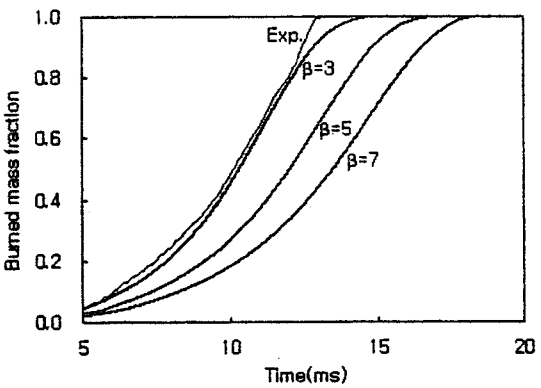

Fig. 6 Effect of the parameter β on burned mass fraction

increased drastically. The results shows that the flame is in the corrugated flamelet regime except the ignition timing of the high swirl case. Since the corrugated flame regime can be included into the wrinkled flamelet regime by extending Klimov-Williams criterion to from Ka=1.0 to Ka=0.1 by Peters (1999), the assumption that the flame is on the wrinkled flamelet regime is thought to be valid.

Different values for α were tried and the results of the burned mass fractions are shown in Fig. 5. The results show that the burned mass fraction agree with the experimental data with α=8. The results of the burned mass fraction for the different value of β are shown in Fig. 6. The flame propagation rate decreases with the increased value of β. Using β=3, the results of the burned mass fraction are similar to the experimental data.

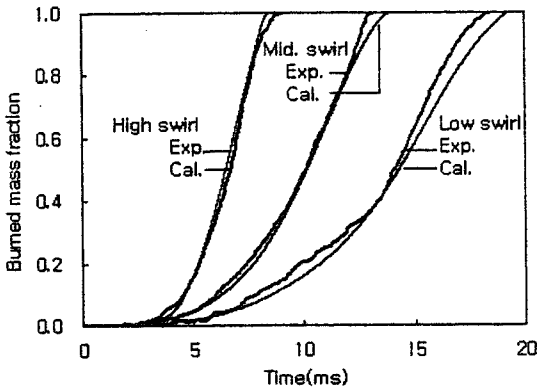

Fig. 7 Effect of the swirl on burned mass fraction

Near the wall, the value of γ_w=2 is chosen to match the experimental results.

The effect of the swirl on the burned mass fraction is shown in Fig. 7 for Re_p=1950, 3435, and 6313. As the swirl strength increases, the burning duration is shortened. The effect of the swirl on the flame surface density distribution is clearly visible because of the capacity of the FSD model to calculate the increased flame propagation due to turbulence.

3.2 Interaction between flow and flame

Figures 8-10 show the computed and measured flame propagation (Lee et. al. 2000) under various swirl strengths (RE_p=1950, 3435, and 6313). Lee et. al. visualized plasma jet ignited flame propagation in a swirling combustion chamber using the schlieren technique. The conventional spark ignition case was compared with the computed result by favor of Lee. Because the schlieren photographs reflect the density gradient, the flame is presented as a constant density line on a plane at z=1.25mm. Figure 8 shows flame propagation under the low-swirl (RE_p=1950) condition. The flame propagates counterclockwise. The flame is decreased at the wall because of the boundary layer and a quenching effect at the cold wall. Figure 9 shows the flame propagation under the medium swirl (RE_p=3435) condition. The flame speed under medium swirl is faster than the low swirl case. Figure 10 shows the flame propagation under the high swirl (RE_p=6313) condition. Although the computed results cannot show the

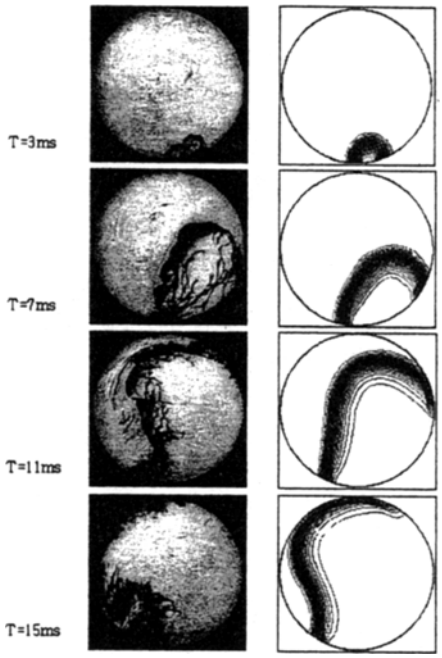

Fig. 8 Comparison of the flame propagation under low-swirl between experiment and computed results

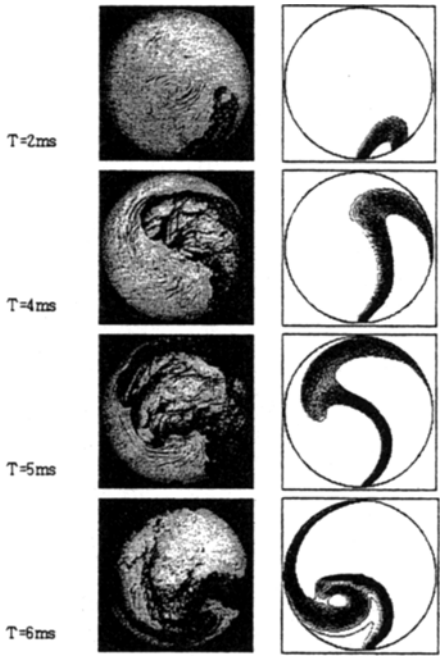

Fig. 10 Comparison of the flame propagation under high-swirl between experiment and computed results

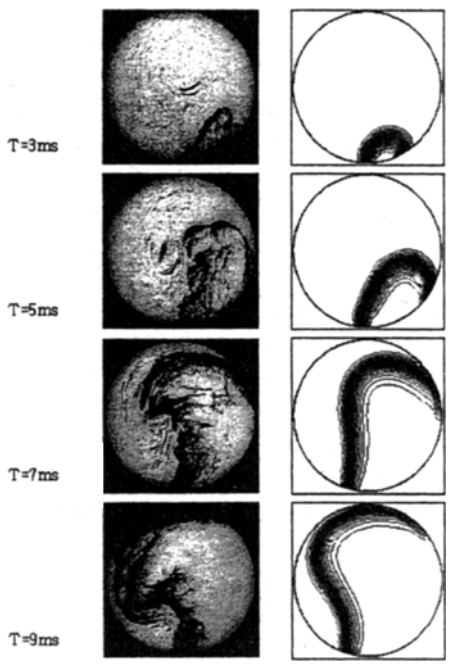

Fig. 9 Comparison of the flame propagation under medium-swirl between experiment and computed results

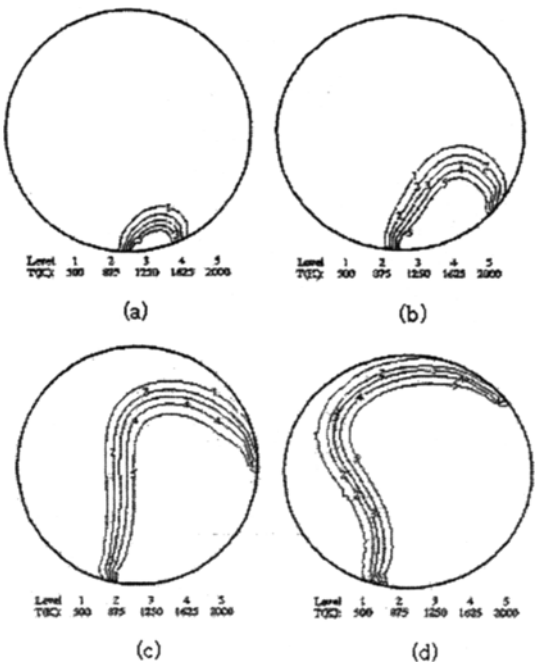

Fig. 11 Temperature contour at different time, (a) t=3ms, (b) t=5ms, (c) t=7ms, (d) t=9ms

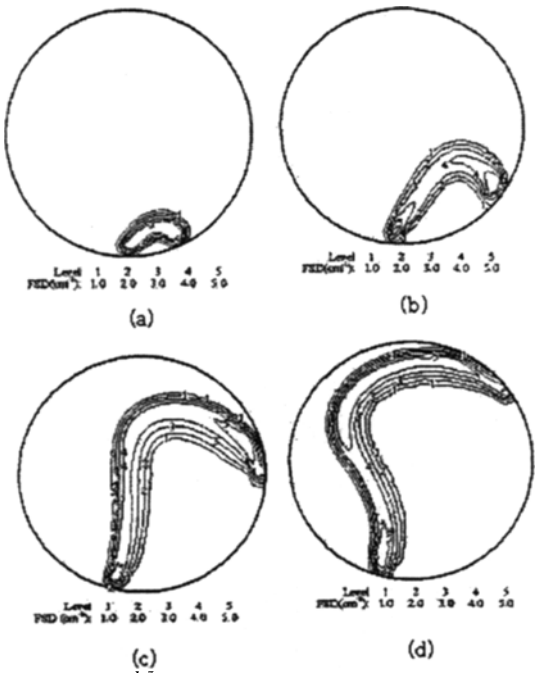

Fig. 12 Flame surface density contour at different time, (a) t=3ms, (b) t=5ms, (c) t=7ms, (d) t=9ms

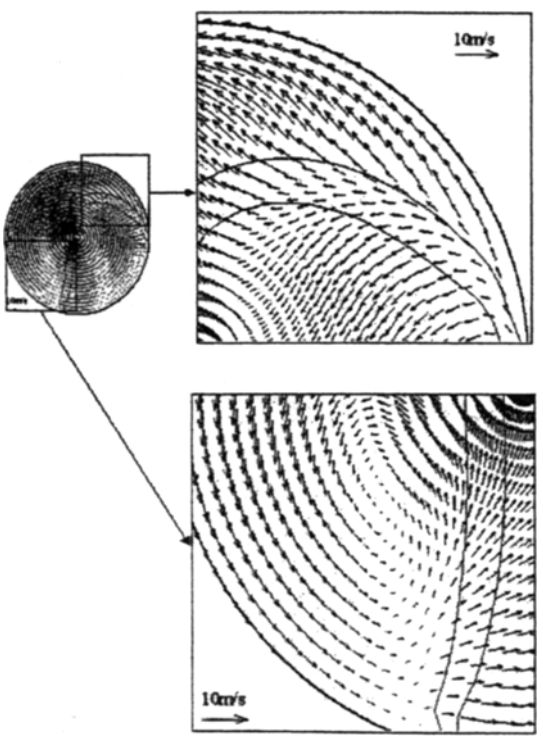

Fig. 13 Velocity vector field across the flame front

Figure 11 shows the temperature distribution under the mid-swirl condition. The temperature distribution matches with the flame surface density distribution in Fig. 12. Between t=3ms to t=9ms, the initial temperature (313K) of the burned gas increases by 200K due to heat transfer and compression of unburned gas by the flame. Figure 12 shows distribution of the flame surface density under the mid-swirl condition. The thickness of flame surface density region is increased as 1-2cm during the propagation. Figure 13 shows distribution of the velocity under the mid-swirl at t=7ms. In the upper-right region, the flame collides with the swirl. However, in the lower-right region, the flame collides with the swirl and forms a smooth curve.

4. Conclusion

A FSD model was applied to KIVA-3V to predict propagation of turbulent premixed flames. The combustion characteristics of turbulent premixed flames in a swirl flow were investigated and compared with experimental data. The results are summarized as follows.

(1) The FSD model was applied with the flames assumed to be in the wrinkled flamelet regime. The calculated results showed that the flame in this study was in the corrugated flamelet regime which could be included in the wrinkled flamelet regime.

(2) The results from the FSD model were sensitive to the parameters of α, β, and γ_w. These values should, threfore, be calibrated aganst the experimental data.

(3) The flame front expanded toward the swirl direction the flame surface density decreased after burning. As the flame propagates, it increased the turbulent intensity which caused a faster combustion rate. The propagation speed was much enhanced by the swirl flow.

(4) The near-wall model suggested in this study is phenomenological rather than theoretical. However it shows good results in comparison with the experimental photos in vicinity of the wall.

Acknowledgement

This work was supported by grant No. 2001-1-30400-009-2 from the basic research program of the Korea Science & Engineering Foundation.

References

Amsden, A. A., 1997, "KIVA-3V: A Block Structured KIVA Program for Engines with Vertical or Canted Valves," Los Alamos National Laboratory report No. LA-13313-MS

Bray, K. N. C. and Peters, N., 1994, *Turbulent Reactive Flows*, P. A. Libby and F. A. Williams, Eds, Academic Press, San Diego, pp. 66~113.

Cant, R. S., Pope, S. B. and Bray, K. N. C., 1990, "Modeling of Flamelet Surface to Volume Ratio in Turbulent Premixed Combustion," *23rd Int. symp. on combustion, The Combustion Institute*, Pittsburgh, pp. 809~815.

Cheng, W. K. and Diringer, J. A., 1991, "Numerical Modeling of SI Engine Combustion with a Flame Sheet Model," SAE Paper No. 910268.

Choi, C. R. and Huh, K. Y. 1998, "Development of a Coherent Flamelet Model for a Spark Ignited Turbulent Premixed Flame in a Closed Vessel," *COMBUSTION AND FLAME* 114, pp. 336~384.

Duclos, J. M., Veynante, D. and Poinsot, T., 1993, "A Comparison of Flamelet Models for Premixed Turbulent Combustion," *COMBUSTION AND FLAME* 106, pp. 101~117.

Lee, J. H., Park J. S., Yoo H. S. and Kim, M. H., 2000, "Combustion Characteristics by means of Plasma Jet Ignition for Swirl Velocity in the Constant Volume Vessel," *Spring Conference Proceeding, KSAE*, pp. 104~109.

Mantel, T. and Borghi, R., 1994, "A New Model of Premixed Wrinkled Flame Propagation Based on a Scalar Dissipation Equation," *COMBUSTION AND FLAME* 96, pp. 443~457.

Marble, F. E. and Broadwell, J. E., 1977, "The Coherent Flamelet Model for Turbulent Chemical Reactions," Project Squid, Technical Report TRW-9-PU

Metghalchi, G. E., Keck J. C., 1996, "Burning Velocity of Methane-Air Mixtures," *COMBUSTION AND FLAME*, 19: pp. 191~210.

Peters, N., 1999, "The Turbulent Burning Velocity for Large-Scale and Small-Scale Turbulence," *J. Fluid Mech.* 384, pp. 107~132.